Micro-Raman depth analysis of residual stress in machined germanium

R. G. Sparks, W. S. Enloe, and M. A. Paesler
The Department of Physics and the Precision Engineering Center, North Carolina State University, Raleigh, NC, USA

Raman spectroscopy has proved to be a useful nondestructive technique for measuring residual stresses in semiconductors. The Raman microprobe is used to investigate the effects of machine parameters on residual stresses in single point diamond turned germanium (Ge). A profiling technique that provides a method of obtaining the residual stress information as a function of depth with depth resolutions of 10.0 nm is discussed. This method is used to analyze the asymmetrically broadened and shifted spectral features in the machined samples. Residual stresses are sampled across ductile feed cuts in (100) Ge wafers, which were single point diamond turned using various feed rates (12.5, 25 nm/rev), rake angles (0°, −10°, −30°), and clearance angles (6°, 16°). In general a region of plastically deformed material that shows slight compressive stresses exists near the surface of the diamond turned sample. The compressive surface stress increases to a maximum at a depth of ≈50 nm beneath the surface at which point the stress rapidly changes sign. The rapid sign change is indicative of the transition from plastic to elastic deformation. Deeper probe regions exhibit increasing tensile stresses, which reach a maximum and then relax to zero at greater depths in the sample. A related study of the stress field occurring around Vicker's hardness indents provides a link between theoretical and experimental stress profiles and demonstrates the accuracy of the micro-Raman profiling technique.

Keywords: *micro-Raman, depth profiling, residual stress*

Introduction

Raman spectroscopy has been proved to be a widely useful technique for the measurement of a broad range of material properties.[1] For example, Raman spectra are often sensitive to strain and can thus be used as a nondestructive probe of the residual stress. Micro-Raman spectroscopy has been used to measure residual stresses in machined surfaces with a lateral resolution near the diffraction limit.[2] We have extended this technique to incorporate axial resolution (depth into the sample) by the use of several excitation wavelengths, which, by virtue of their differing characteristic penetration depths, allow the determination of stress profiles as a function of depth into the sample. Greater and greater depths in the material may be probed by using successively longer wavelengths of light, thus leading to a superposition of a continuum of Raman peaks. Depth profiles of residual stress can then be obtained using computer deconvolution of the resulting Raman spectra.[3] The present study involves measurement of residual stresses in ductile feed cuts in (100) germanium wafers, which were single point diamond turned using a variety of feed rates, rake angles, and clearance angles. The resulting depth profiles of the residual stresses demonstrate important differences in the stress field for the various machine parameters.

We also map the residual stress fields surrounding Vicker's hardness indents in Ge using the techniques of micro-Raman spectroscopy and computer deconvolution. It is well known that the response of solids to indentation has provided information about phenomena such as erosion, wear, machining damage, and surface fracture strength. A considerable amount of experimental data exists that shows variations of indentation microhardness with load, temperature, and surface contact environment.[4] The magnitude of the elastic-plastic stress field as well as the extent of

Address reprint requests to Dr. M. A. Paesler, Department of Physics, North Carolina State University, Box 8202, Raleigh, NC 27695-8208.

plasticity are of primary importance to the indentation fracture process. The theory of rigid perfectly elastic solids can be used to predict indentation pressures, using wedge-shaped or conical indenters, which depend only on the geometry of the indenter and the yield stress of the material.[5] Since Vicker's hardness indents produce stress fields that are better empirically understood than the machined samples, important insights into the material removal process can be obtained from the comparison of indents with diamond turned samples. In addition, since the stress fields in the vicinity of Vicker's hardness indents are well modeled, probes of the surrounding stress field can provide a conclusive verification of the validity of our Raman profiling technique.

Experiment

Raman spectroscopy involves two photons: one incident photon that excites the effect and one scattered photon that is collected and analyzed. The scattered light spectrum will exhibit peaks at some characteristic frequency shift from the excitation photon frequency.[2] The excitation source consists of an argon ion laser with strong outputs at 514.5 and 488.0 nm. The light from the laser is plane polarized in a direction normal to the plane formed by the optical table on which the laser is mounted. The plane polarized, monochromatic beam is then steered using plane mirrors through an achromatic halfwave plate (Fresnel rhomb). The effect of the halfwave plate is to rotate the polarization state of the excitation beam by a known angle with respect to the original polarization state. Since the Fresnel rhomb introduces some ellipticity in the emerging beam, a Glan-Thompson prism polarizer mounted to a calibrated rotation stage is used to provide a pure linear polarization state at a known angle (*Figure 1*). The light is then steered into the micro-Raman apparatus (SPEX Micramate) where the known polarization state is focused by a 40 × microscope objective onto the sample with a particular orientation to the sample's crystal direction. The microscope objective collects the scattered light, but, since the excitation beam is incident normally onto the sample, the specularly reflected beam is collected as well. The scattered and reflected light is then focused by the coupling optics on the entrance slit of a double Czerny-Turner 0.85-m holographic grating spectrometer (SPEX 1403) where the collected light is dispersed. In order to increase stray light rejection the dispersed light is then passed into a third monochromator stage (SPEX 1442U), which functions as an additional spectral filter. The rejection of stray light provided by the third monochromator stage for micro-Raman spectroscopy (where the specularly reflected beam cannot be geometrically rejected) becomes critical, especially for materials with Raman spectral features close to the exciting laser line. The resulting Raman spectra typically

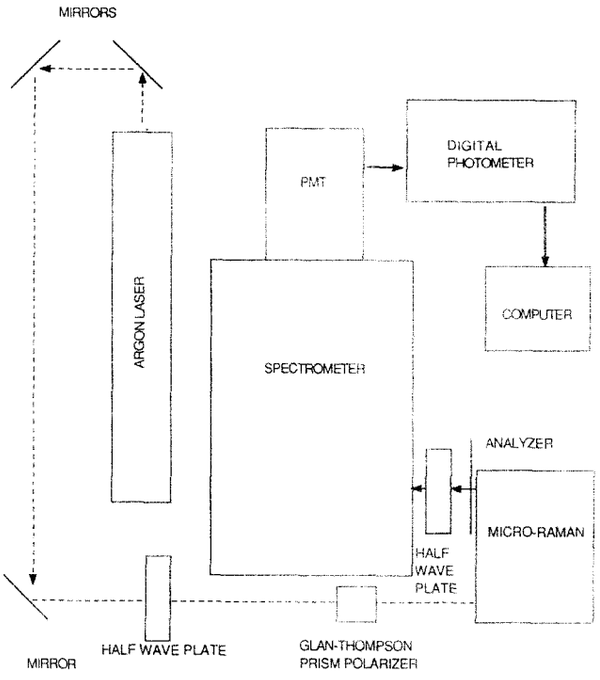

Figure 1 Experimental apparatus. The Raman effect is excited using the Ar laser. The polarization of the laser light is rotated by the half-wave plate. Backscattered light is collected by the micro-Raman apparatus, with dispersion of the scattered light accomplished using the spectrometer. Photon counting is performed by the PMT and photometer. Photon counts as a function of frequency are recorded by the computer.

exhibit asymmetrically broadened peaks, which result from the superposition of a continuum of stress states as the sample probe depth is increased. Deconvolution of the resulting asymmetrically broadened Raman spectra yields depth profiles of the residual stresses in the single point diamond machined samples.

When light of intensity I_0 penetrates a solid, the intensity, I, at any depth z will be given by

$$I = I_0 e^{-\alpha z} \qquad (1)$$

where α is the absorption coefficient and $1/\alpha$ defines a characteristic depth for light in the sample known as the penetration depth. In the case of Raman scattering, the light must penetrate to a depth z before being scattered, and it must return to the surface in order to be collected; therefore, the intensity of the Raman signal from any depth, z, will be proportional to $e^{-2\alpha z}$ (the absorption coefficient for the scattered light is actually slightly different from that of the incident light; these slight variations will not be considered). The value of the absorption coefficient depends on both the material of interest and the energy of the incident light. The behavior of the absorption coefficient[6] versus energy for silicon,

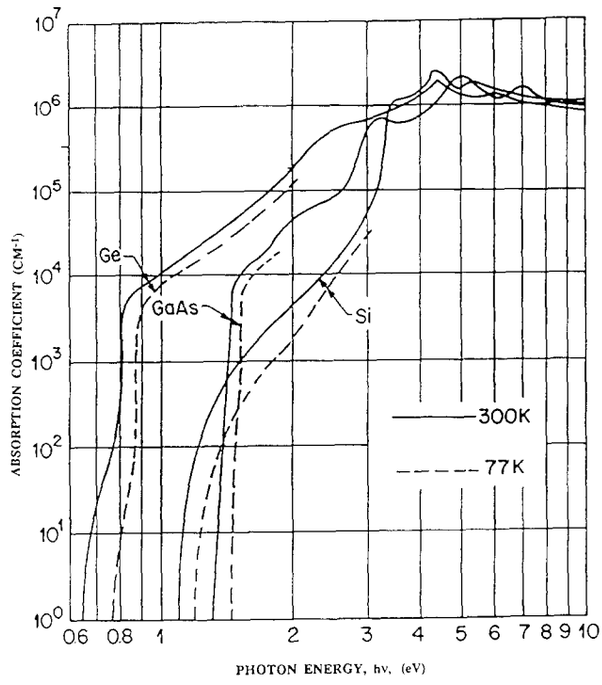

Figure 2 Absorption coefficient as a function of photon energy. The absorption coefficients for Si, Ge, and GaAs are plotted as a function of incident photon energy.[6] Light from the Ar laser lies in the range between 2 and 3 eV.

Ge, and gallium arsenic demonstrates the material and wavelength dependences (*Figure 2*). The exponential decay of the intensity of the Raman signal with depth combined with the variation of the absorption coefficient with photon energy makes determination of stress profiles from Raman spectra in opaque semiconductors possible.

Initial depth profiles were generated from Raman scattering data obtained using the green (514.5 nm) and blue (488 nm) lines of an argon ion laser with energies near 2.5 eV. In this region the absorption coefficient shows different behavior for the different materials. For Si, the absorption coefficient, and therefore the penetration depth, is rapidly changing over this region, but it is relatively low. In Si, green light would have a penetration depth of just under 1 μm. Ge, on the other hand, has a much higher absorption coefficient. Green light has a penetration depth of approximately 0.15 μm in Ge. The disadvantage is that the absorption coefficient changes very slowly with energy over this range. The absorption coefficient of GaAs is intermediate between that of Si and Ge, and it varies either rapidly or slowly, depending on the exact energy of the light used. The absorption coefficient, or alternatively the penetration depth, of the light used determines the effective volume sampled by the Raman signal. Thus, by adjusting the energy of the light used it is possible to study the variation of stress over different depths in the material. Another important consideration is that when the absorption coefficient is changing rapidly with energy, it may no longer be valid to assume that the absorption coefficient is the same for the incident and the inelastically scattered light.

It can be assumed that to first order the Raman signal has a Gaussian lineshape. Thus, the analytical expression for the Raman signal, $R(\omega)$, is

$$R(\omega) = A \int \exp[-2\alpha z] \exp\left[\frac{-(\omega - \omega_z)^2}{2\sigma^2}\right] dz \tag{2}$$

where $\omega_z = \omega_0 + S(z)$. This expression consists of an integral over all depths and contains an exponential decay that modifies the assumed Gaussian lineshape. The Gaussian lineshape is located at angular frequency ω_z and has an associated natural line width $2\sigma^2$. The amplitude factor, A, is included to scale the integral to the measured Raman data. The depth dependence, z, enters expression in the exponentially decaying intensity factor and in ω_z. The term ω_z gives the location of the unshifted Raman signal, ω_0, plus the shift due to the stress at each incremental depth dz. This shift function, $S(z)$, will hereafter be referred to as the stress profile.

A depth, z_0, is chosen such that beyond this depth the stress may realistically be presumed to vanish. The integral in the Raman function is naturally divided into two regions, greater and less than z_0. Where the stress is zero ($z > z_0$), the Gaussian lineshape can be taken outside the integral, and the remaining integral can easily be solved analytically. For $0 < z < z_0$, the stress is changing and the integral can only be solved numerically. Numerical integration involves dividing the interval into dz elements and then evaluating the function at each z. Therefore, the stress function, $S(z)$, must be evaluated at each z regardless of its functional form. The stress at each depth can then be made a parameter that is free to vary. The function to be fitted then becomes

$$\begin{aligned} R(\omega) = &\sum_j A \exp[-2\alpha z_j] \\ &\exp\left\{\frac{-(\omega - [\omega_0 + S(z_j)])^2}{2\sigma^2}\right\} dz \\ &+ \frac{A}{2\alpha} \exp[-2\alpha z_0] \exp\left\{\frac{-(\omega - \omega_0)^2}{2\sigma^2}\right\} \\ &+ bk \end{aligned} \tag{3}$$

The first term is the integral over a depth of zero to z_0 of the assumed Gaussian lineshape. The second term is the integral of the Gaussian lineshape from a depth z_0 to infinity and is constant for a given value of z_0. An additional term, bk, allows for a background correction. The only parameters free to vary are the $S(zj)$s, the residual stresses at each

depth; thus, the stress profile can assume any form, even if it is discontinuous.

Least squares data analysis involves minimization of the sum of the squares of the differences between the experimental and the calculated data. This sum of squares is referred to as χ^2 and

$$\chi^2 = \sum \frac{(Y_{exp} - Y_{fit})^2}{\eta^2} \quad (4)$$

where η^2 is the experimental uncertainty associated with each data point. Since the Raman data are collected in a photon-counting mode, the data follow Poisson statistics[7] and the uncertainty, η, is equal to the square root of the number of counts (typically $\eta \leqslant 0.01$ near the Raman peak). The interval from zero to z_0 is divided into an appropriate number of intervals, each having width dz. The Raman function is approximated by the above sum, and the stress at each depth is varied until the calculated Raman signal corresponds to the one obtained experimentally by minimization of χ^2.

χ^2 is a function of the experimental uncertainties and the parameters $S(z_j)$. These parameters span a j dimensional space known as parameter space. There are a number of standard methods[7] for minimizing the function χ^2, which involve searching parameter space for the smallest value of χ^2. A grid search least squares technique is employed that involves the independent variation of each parameter, $S(z_j)$, until χ^2 is minimized. The next parameter is then adjusted, following a grid in parameter space. This procedure is repeated until the incremental change in χ^2, $\Delta\chi^2$, is less than some specified value (typically 1%). The disadvantage of this method is that convergence is very slow since each parameter is adjusted independently while holding all the others constant. It is also implicitly assumed that the various χ^2s are optimal or near optimal. In the initial stages of the fit (i.e., far from the minimum χ^2), this is not the case and this effect contributes to the slow convergence of this method.

A significant problem associated with optical measurements of depth profiles is that the intensity is a maximum at the surface and decays exponentially into the sample. This makes optical measurements subject to cumulative errors traceable to the surface data.[8] In addition, the absorption coefficient (penetration depth)[6,8] is sensitive to the defect density, band structure, and doping level of the sample, particularly near the absorption edge. The ability to adjust the penetration depth of the light is therefore often severely limited by the absorption coefficient versus energy curve and the availability of appropriate laser lines. Data from several laser lines can often be used to make qualitative estimates of the residual stresses; with the high penetration depth (longer wavelength) data providing bounds on the stress profile deep in the material while the low penetration depth (shorter wavelength) data is used to determine the nature of variations near the surface. The criterion for a good fit is determined by minimizing χ^2. If data are taken with green and blue laser lines, it is possible to define a χ^2_{blue} and χ^2_{green} to measure the deviations from the blue and green data, respectively. The simplest solution to this problem would be to minimize the total χ^2 defined as the sum of χ^2_{blue} and χ^2_{green} or

$$\chi^2_{tot} = \chi^2_{blue} + \chi^2_{green} \quad (5)$$

A typical stress profile obtained from machined Ge using the technique described previously is shown (*Figure 3*). The upper plot displays the spectra obtained with blue light (488 nm) and green light (514.5 nm), and the lower plot is the stress profile. The depth resolution of this technique is determined by the distance between the $S(z_j)$s. A value of 6 nm is typically used for this spacing and changes in the residual stress have been observed over this scale, indicating that this value is a good

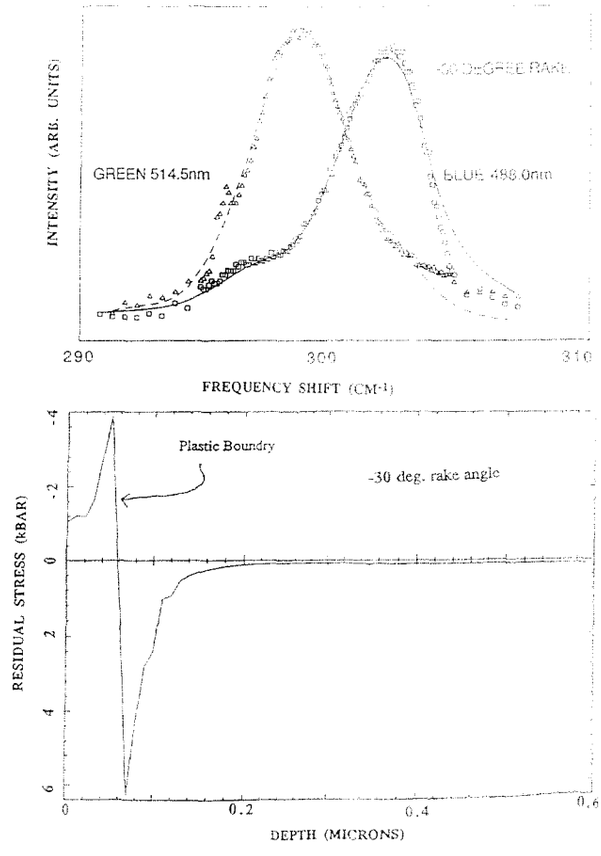

Figure 3 Raman peaks and an associated depth profile. Raman spectra are obtained using both 488.0 and 514.5 nm excitation wavelengths. The Raman features are shifted from the unstressed frequency ($\approx 300\ cm^{-1}$) and are asymmetrically broadened. The resulting profile of stress as a function of depth is displayed at the bottom of the figure.

upper bound for the depth resolution in this system. The maximum depth resolution for this technique is determined by the value of the absorption coefficient for the light used, with higher absorption coefficients giving greater depth resolution. It has been shown that when the stress is changing over the volume sampled, it is inappropriate to determine the magnitude of the stress from the peak value of the Raman signal alone.

Results

The depth profiling technique has been used to evaluate the effect of machine parameters on the residual stress states in single point diamond turned Ge. Machine parameters such as feed rate (12.5 and 25 nm/rev) and spindle speed (1,000 and 2,500 rpm) ($-10°$ rake angle, 6° clearance angle for all cases) showed few differences in their spectra, and the resulting surface stresses are always compressive. The depth at which the transition from compressive to tensile stress is evident is approximately constant for all feed rates and spindle speeds used and occurs at a depth of 60.0 ± 10.0 nm. Our results indicate that the effects of these particular feed rates and spindle speeds on the residual stress field are not significant. Further investigation using a wider range of feed rates and spindle speeds is therefore indicated to more fully understand the effects of these parameters. Quite marked differences are evident, however, in the case of rake and clearance angles. Ge samples turned using 0°, $-10°$, and $-30°$ rake angles (all with 25 nm/rev feed rate, 1,000 rpm spindle speed, 60–125 nm depth of cut, 6° clearance angle) show clear evidence of superposition broadening with significant variations in the spectra obtained using 514.5- and 488.0-nm probes. These differences indicate changes in both the magnitude of the residual surface stresses and the depth at which the stress changed from compressive to tensile. Models of stress obtained from hardness indents associate such rapid sign changes with a transition from a plastic to elastic deformation zone.[5] Differences in the maximum magnitudes of the compressive and tensile stresses were also noted in the samples under consideration.

The depth profiles generated for the 0° and $-30°$ rake angles display similar behavior in the magnitudes of the compressive stress at the surface of the sample (*Figure 4*). In both cases the compressive surface stress increases to a maximum value at depths of ≈ 50 nm. The maximum magnitude of the compressive stress is seen to be larger for the $-30°$ rake angle, and the stress penetrates to greater depths than in the case of the 0° sample. In both cases the magnitude of the stress rapidly changes sign, which results in a discontinuity in the measured stress profile. The depth at which this discontinuity occurs is indicative of the transition from plastic to elastic deformation

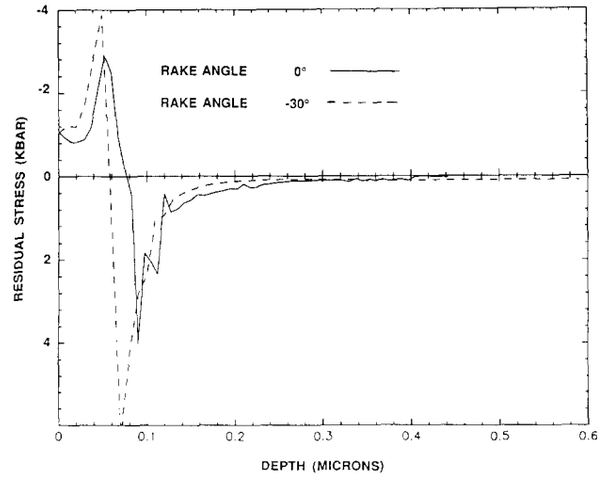

Figure 4 Depth profiles for 0° and $-30°$ rake angles. Residual stress as a function of depth is plotted for each rake angle. The plastic-elastic transition boundary is clearly evident.

and is seen to be slightly different for these rake angles. It should also be noted that the maximum magnitude of the tensile stress is again greater for the $-30°$ rake angle but this stress penetrates to a shallower depth than the tensile stress field measured for the 0° rake case. The tensile stress is observed to relax smoothly to zero, with the stress vanishing at depths of ≈ 40 nm. Raman spectra obtained using the 514.5- and 488.0-nm probe wavelengths on Ge samples turned with a $-6°$ rake angle showed significant differences in their shifts and asymmetries. The resulting stress profile indicates that again there exists a comprehensive stress near the surface of the material with the magnitude of this stress greater than either the 0° or $-30°$ rake angle cases. The behavior of the compressive surface stress as a function of depth is markedly different for the $-10°$ rake angle, however. The compressive surface stress is seen to decrease gradually until a depth of ≈ 50 nm is reached at which point the compressive stress rapidly increases to a magnitude significantly greater than the maximum compressive stress observed for either of the two other rake angles studied. The stress then rapidly reverses sign, reaching a maximum magnitude of tensile stress intermediate between the magnitudes of tensile stress measured for the 0° and $-30°$ rake angle cases. The penetration depth of this tensile stress is also found to lie between the depths measured for the 0° and $-30°$ rake angle cases. A smooth relaxation to zero stress was not observed for the $-10°$ rake angle; the spectra showed evidence of a broad region of slowly varying tensile stress between depths of 15.0 and 25.0 nm. A smooth relaxation to zero stress is then observed for greater depths (*Figure 5*). It should be noted that the existence of the sharp

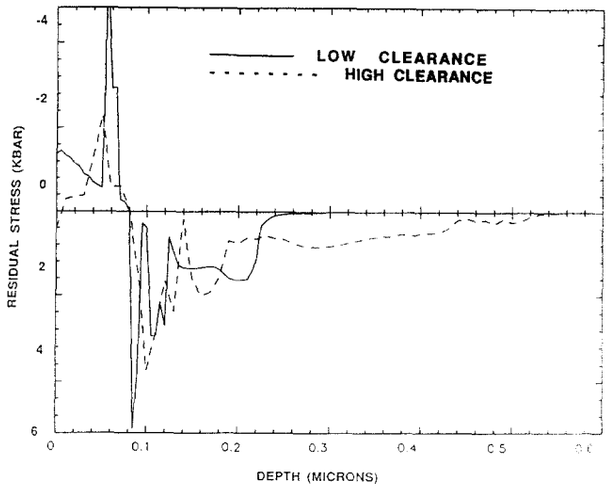

Figure 5 Depth profile for −10° rake angle, low clearance and high clearance. The same general behavior as at 0° and −30° rake angles is seen; however, the secondary tensile peaks are quite different. Note that the stress field for the high clearance angle tool penetrates more deeply than the low clearance case.

secondary tensile peaks observed for the −10° rake angle (both low and high clearance cases) may be due to numerical instabilities in the deconvolution program and do not necessarily reflect actual physical changes. The general shape of the profile and the magnitude of the major features are reproducible however.

The effects of standard and high clearance angles (6° and 16°, respectively) were also investigated (−10° rake angle, 6–125 nm depth of cut, 25 nm/rev feed rate, 1,000 rpm spindle speed). The effects of −10° rake angle with a 6° clearance angle were discussed previously. The use of the same machine parameters with a clearance angle of 16° resulted in a depth profile of the residual stress similar to the low clearance case but with subtle differences. The measured depth profiles indicate that a slightly tensile stress exists near the sample surface. The stress changes sign and increases to a maximum compressive stress of lower magnitude than any of the other cases studied. The stress again changes sign building toward a maximum tensile stress comparable to the 0° and −30° rake angle cases. Secondary peaks in the tensile stress were observed as in the case of the −10° rake angle (6° clearance angle) case, which again may be attributed to numerical instabilities. A broad region of slowly varying tensile stress was again measured, although in this case the stress penetrates much more deeply into the sample (*Figure 5*). *Table 1* lists the magnitudes of the surface stresses and compressive and tensile maxima for the various rake angles studied. *Table 2* displays the depths of the stress maxima and plastic-elastic transitions in the sample.

Initial studies of Vicker's indents have generated depth profiles that confirm the validity of the depth profiling technique as an accurate means of determining the depth variation of stress in opaque samples. Depth profiles obtained for radial probe distances of 5 and 10 μm from the dent center (*Figure 6*) show a region of compressive stress near the surface of the material that is indicative of a plastically deformed zone. The regions underlying this plastically deformed zone exhibit tensile stresses that are expected for the region of induced elastic deformation that accompanies the plastically deformed zone. The depth at which the transition from plastic to elastic deformation is clearly seen to vary directly with the radial distance from the dent center, which is to be expected for the hemispherical zone of compressive stress associated with Vicker's hardness indents. Since the Raman scattering tensor displays different polarization states with respect to both the excitation polarization and the crystallographic directions in the sample, an analyzer placed in the Raman scattered light is used to select a particular known polarization state. Computer deconvolution techniques are used to generate depth profiles of the stress field for each polarization state studied. It has been found from initial polarization studies that certain forbidden Raman polarization states are observed in the vicinity of the Vicker's hardness indents. This indicates a destruction of the perfect crystal symmetry by the application of a nonisotropic stress field. A complete analysis of the stress tensor is

Table 1 Characteristic depths and magnitudes of stresses for machined germanium

Rake angle	Depth of maximum compressive stress (nm)	Depth of maximum tensile stress (nm)	Depth of plastic-elastic transition (nm)	Surface stress magnitude (GPa)	Maximum compressive stress (GPa)	Maximum tensile stress (GPa)
0°	60.0 ± 10.0	90.0 ± 10.0	70.0 ± 10.0	11.0 ± 1.0	35.0 ± 1.0	48.0 ± 1.0
−10°	60.0 ± 10.0	80.0 ± 10.0	70.0 ± 10.0	18.0 ± 1.0	73.0 ± 1.0	61.0 ± 1.0
−30°	40.0 ± 10.0	70.0 ± 10.0	60.0 ± 10.0	13.0 ± 1.0	48.0 ± 1.0	73.0 ± 1.0

Table 2 Characteristic depths of stress maxima, plastic-elastic transition and for 0°, −10°, −30° rake angles

Rake angle	Depth of maximum compressive stress (microns)	Depth of maximum tensile stress (microns)	Depth of plastic-elastic transition (microns)
0°	0.06 ± 0.01	0.09 ± 0.01	0.07 ± 0.01
−10°	0.06 ± 0.01	0.08 ± 0.01	0.07 ± 0.01
−30°	0.04 ± 0.01	0.07 ± 0.01	0.06 ± 0.01

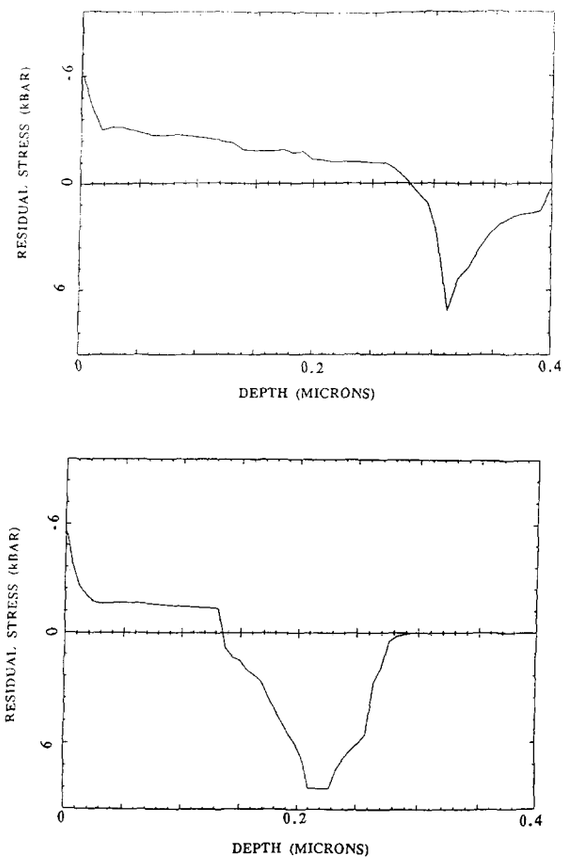

Figure 6 Depth profiles generated from the residual stress field around Vicker's hardness indents. The top profile was obtained at a point ≈5 μm from the dent edge. The zone of compressive stress penetrates to ≈30 nm into the sample. The lower profile was obtained at a radial distance of ≈15 μm from the dent edge. The compressive zone is clearly seen to penetrate to a smaller depth (≈15 nm).

underway. Considerable data must be taken at each position on the sample to measure the second rank stress tensor components, with each component requiring two spectra (of different polarization orientations) for each wavelength. In order to improve convergence time of the depth profiling technique, four wavelengths (514.5, 496.5, 488.0, and 476.5 nm) are now used to obtain high-quality depth profiles for each polarization orientation. Further computer modeling will be required to fully understand the interaction of the symmetries of the Raman scattering and applied stress tensors.

Conclusions

Micro-Raman spectroscopy coupled with the use of computer deconvolution of the resulting spectra has yielded a wealth of information concerning the effects of machine parameters on the residual stress field in single point diamond turned Si and Ge. It has been found from our investigations that for the feed rates and spindle speeds studied that no significant variations in the residual stress field are noted. All feed rates and spindle speeds examined in our study resulted in a compressive surface stress that showed a rapid increase to maximum values of ≈30 GPa at a depth of ≈50 nm. The magnitude of the stress then changes sign and reaches a maximum tensile stress of approximately the same magnitude at a depth of ≈70 nm. Significant variations in the stress field were noted, however, for the various rake and clearance angles studied. These variations seem to indicate changes in both the magnitude of the surface stress as well as significant variations in the region of plastic-elastic transition in such samples.

Acknowledgments

We would like to thank the faculty and students of the Precision Engineering Center at North Carolina State University for providing helpful discussions and encouragement. This work was supported under the auspices of the Office of Naval Research contract N00014-83-K-0064, with additional contributions from the industrial affiliates of the Precision Engineering Center of North Carolina State University.

References

1 Nemanich, R. J. *Mat Res Soc Symp Proc* 1986, **69**, 23–27
2 Sparks, R. G. *Prec Eng* 1988, **6**, 191–198
3 Sparks, R. G. *Microbeam Analysis–1989*, 1989, 149
4 Chaing, S. S., Marshall, D. B., and Evans, A. *J Appl Phys* 1982, **53**, 298
5 Johnson, K. L. *J Mech Phys Solids* 1970, **6**, 75
6 Sze, S. M. *Physics of Semiconductor Devices*, New York: John Wiley and Sons Inc., 1981
7 Bevington, P. R. *Data Reduction and Error Analysis for the Physical Sciences*, New York: McGraw-Hill, 1969
8 Pankove, J. I. *Optical Processes in Semiconductors*, New York: Dover Publications, Inc., 1971